3D Electromagnetic Modeling of Parasitics and Mutual Coupling in EMI Filters

Ivana F. Kovačević, *Student Member, IEEE,* Thomas Friedli, *Member, IEEE,* Andreas M. Müsing, *Student Member, IEEE,* and Johann W. Kolar, *Fellow, IEEE*

***Abstract*—The Electromagnetic Compatability (EMC) analysis of Electromagnetic Interference (EMI) filter circuits using 3D numerical modeling by the Partial Element Equivalent Circuit (PEEC) method represents the central topic of this paper. The PEEC-based modeling method is introduced as a useful tool for the prediction of the high frequency performance of EMI input filters, which is affected by PCB component placement and self- and mutual-parasitic effects. Since the measuring of all these effects is rather difficult and time consuming, the modeling and simulation approach represents a valuable design aid before building the final hardware prototypes. The parasitic cancellation techniques proposed in literature are modeled by the developed PEEC-Boundary Integral (PEEC-BIM) method and then verified by the transfer function and impedance measurements of the *L-C* and *C-L-C* filter circuits. Good agreement between the PEEC-BIM simulation and the measurements is achieved in a wide frequency range. The PEEC-BIM method is implemented in an EMC simulation tool, GeckoEMC. The main task of the presented research is the exploration of building an EMC modeling environment for virtual prototyping of EMI input filters and power converter systems.**

***Index Terms*—Electromagnetic Interference (EMI) filter, 3D electromagnetic modeling, Partial Element Equivalent Circuit (PEEC) method, parasitics, mutual coupling, parasitic cancellation techniques, virtual prototyping.**

Note: This paper has never been published in other conferences or journals and it has been fully edited to its submission for consideration to the IEEE Transactions on Power Electronics.

I. Introduction

To meet Electromagnetic Compatibility (EMC) regulations, power electronic devices have to be designed with respect to EMC standards for High Frequency (HF) Electromagnetic Interference (EMI) noise emission and susceptibility. EMC standard requirements defined by European or USA regulations for a wide-range of applications, e.g. CISPR and FCC [1], have to be considered in the earliest design stages in order to satisfy market demands on time with high-quality performance. Therefore, there is an ever-increasing interest in efficient EMI mitigation techniques and EMI/EMC modeling and simulation tools enabling the prediction of the electromagnetic behavior prior to the final hardware implementation.

The well-known cause of EMI problems in power electronics is fast switching of high currents and voltages within the power converter systems. The EMC compliant power electronics must fulfill the limits for both conducted and radiated EMI noise levels. It has been shown that the EMI mitigation techniques at the noise-source-side such as soft-switching techniques [2], different modulation schemes [3], improvement of high-frequency behavior of switching devices [4] etc., can reduce the generation of EMI noise by up to approximately $5-10\,\mathrm{dB}$, but the main improvements come from the employment of proper EMI design, EMI filtering, and shielding measures [5]. The EMI radiation problems can be eliminated to the required extent by adequate layout and shielding techniques, and EMI filters has to be used in order to decrease EMI conduction noise. Additionaly special care must be taken concerning more sophisticated electromagnetic effects including components' parasitic effects, mutual coupling, wiring, PCB layout, grounding, etc. The aim of EMI filters is to attenuate the conducted noise signals exiting the power electronic device and propagating through the AC power lines and to the surrounding equipment. Conventional EMI filtering is achieved by passive power line filters interfaced between power lines and Switched Mode Power Supplies (SMPS) and do not require complicated control schemes (as is the case with an active filtering approach which is rather used for harmonic filtering). However, the passive EMI filters introduce additional cost and volume and have to be properly designed.

The design of EMI input filters has to be observed as part of the overall design process of power converter systems. A good understanding of EMI noise generation and propagation is necessary for building "good" EMI filter designs and hence EMC analysis represents an important task for power electronic engineers. The design of passive EMI filters has been typically based on rules of thumb which demand great practical experience [6] or based on the analytical methods derived from the equivalent high (HF) circuit description of EMI filter components [7]. The modeling of an EMI filter as a two-port network was described in [8], where the mutual coupling parameters were extracted from the scattering-matrix measurements for the identification and quantitative assessment of self- and mutual-parasitic effects. The main problem of this equivalent HF circuit approach is to define a proper electrical circuit that corresponds to the real physical behavior, and furthermore the complexity of such a circuit can be computationally very expensive.

Manuscript received October 25, 2012, Corresponding author. Ivana F. Kovačević, Tel: +41 44 632 27 69; fax: +41 44 632 12 12 *E-mail address*: kovacevic@lem.ee.ethz.ch, *Mail address*: Physikstrasse 3, ETL H18.1, 8092 Zurich, Switzerland

Ivana F. Kovačević, Andreas M. Muesing and J. W. Kolar are with Power Electronic Systems Laboratory, ETH Zurich, Zurich 8092, Switzerland (e-mail: kovacevic@lem.ee.ethz.ch; muesing@lem.ee.ethz.ch; kolar@lem.ee.ethz.ch). Thomas Friedli is with ABB Switzerland, Ltd., Zurich CH-8050, Switzerland (e-mail: thomas.friedli@ieee.org.).

The selection of EMI suppression components has to be carefully performed taking into account HF phenomena which in turn negatively influence the frequency performance of components. It is shown in [9]–[12] that 3D electromagnetic modeling based on the numerical techniques can provide a comprehensive insight into the electromagnetic behavior of EMI filter components (inductors, capacitors, resistors) and thus, it can be considered as useful tool for the optimization of the EMI filter design procedure [6]. The Partial Element Equivalent Circuit (PEEC) method has been shown to be the most suitable numerical technique for fast and accurate EMC modeling of power converter systems. Accordingly, the main topic of this paper is the EMI/EMC analysis and 3D electromagnetic modeling of the self-parasitic and mutual coupling effects of passive EMI filter components using the PEEC numerical technique. Coupling between two numerical techniques, the PEEC method and the Boundary Integral Method (BIM), i.e. PEEC-BIM method, first proposed in [13], [14] for the detailed electromagnetic modeling of EMI filter inductors, allowes the 3D PEEC-based modeling to become a useful tool for the prediction of the high frequency (HF) performance of EMI input filters and power converter systems. The main aim of this paper is to introduce the developed PEEC-BIM method as a useful approach for the assessment of dominant parasitic effects that determine the HF response of the EMI filters. Since the dominant parasitic effects are a combination of different self- and mutual-parasitic effects, they are hard to analytically calculate and measure. It is shown in this paper that the developed PEEC-BIM method enables a detailed EMC analysis, which simultaneously takes into account different electromagnetic effects of the PCB layout, self parasitics, mutual coupling, electrostatic shielding, and so on. Moreover, it is demonstrated that the developed PEEC-BIM modeling approach implemented in the 3D PEEC-based simulation tool can be used to evaluate the applicability of parasitic cancellation techniques proposed in literature for the efficient cancellation of the self-parasitic and mutual-coupling effects in complete EMI filter circuits.

In **Section II**, the main principles of 3D electromagnetic modeling based on the Partial Element Equivalent Circuit method are described. An extension of the standard PEEC method, the PEEC-Boundary Integral (PEEC-BIM) method was developed to enable modeling of EMI filter inductors. The main feature of the proposed method is the PEEC-based modeling of magnetic components for power electronics that was previously lacking for the implementation of a full 3D PEEC-based EMI/EMC modeling environment. The EMC modeling of EMI filter inductors and capacitors is presented in **Section III**. Some parasitic cancellation techniques proposed in literature were investigated and verified both by the PEEC-based simulation and measurements. Finally, the advantages of using the 3D EMC modeling approach based on the PEEC method for EMI/EMC analysis of EMI filters are summarized in **Conclusions**. In the **Appendix**, the basic PEEC formulas are explained to provide a more complete understanding of PEEC-based 3D electromagnetic modeling.

II. Parasitic Effects of EMI Filters

EMC analysis can be divided in three parts: (1) identification of the EMI sources, (2) finding the critical signal paths and coupling loops, and (3) EMI prevention by means of different EMI mitigation techniques including the design of EMI filters [15]. However, the final task of building an EMI filter cannot be performed independently of the first two steps, especially in the HF range when parasitics start having a significant influence on the EMI filter performance [16].

A. State-of-the-Art

Degradation of EMI filter performance due to parasitic effects has been a topic of interest of a lot of research [8], [16]–[22]. Namely, the equivalent series inductance of filter capacitors (*ESL*) and the equivalent parallel winding capacitance of filter inductors (*EPC*) become dominant over the main electrical properties, i.e. capacitance C and inductance L, respectively. Additionally, the mutual electromagnetic couplings have an impact on the EMI filter performance and have to be minimized simultaneously. These mutual-parasitics originate from the placement of the filter components, PCB layout, and grounding. Consequently, EMI filters with the same topology and selection of filter components can exhibit different insertion loss. With increasing switching frequency and higher power density, the space constraints and constructional effort for building EMI filters become more pronounced, and all parasitic effects have to be considered in much more detail. Even though the presence of self- and mutual-parasitics have been studied a lot over the years, distinguishing and assessing the influence of these effects on the overall HF behavior of EMI filter is still regarded as a complex task.

Neugebauer et al. [17]–[19] proposed different techniques for the self-parasitics cancellation of filter capacitors and inductors. These cancellation techniques were theoretically proven and verified by measuring the frequency response of individual components. The integration of a parasitic inductance cancellation technique into an existing EMI filter was investigated in [19]. However, the demonstrated results represent only one particular example and a more detailed investigation about the practical applicability of these techniques in real EMI circuits is still missing. The work of Wang et al. [8], [16], [20]–[22] covered the main problems introduced by the parasitic effects of EMI filter performance in the HF range. The identification and quantitative assessment of these effects was performed by observing an EMI filter as a two-port network and extracting the mutual coupling parameters from the scattering-matrix measurements in [8]. Furthermore, it was shown by experiments that the self-parasitics cancellation techniques do not introduce significant improvements if the mutual parasitic effects dominate and they are not sufficiently reduced in advance [20]. The cancellation of mutual inductive coupling between EMI filter components was proposed in [21], [22]. The authors analyzed the possibilities to apply different cancellation techniques to a real EMI filter in [20], but only concentrating on EMI filter circuits with regular, i.e. aligned, component arrangements. A general approach to analyze all these properties of EMI filters has not been developed so

far. Accordingly, the motivation of this paper is to introduce 3D electromagnetic modeling as a useful tool for detailed EMC analysis of EMI filters which allows the prediction of all parasitic effects and EMI filter performance in the frequency range of interest defined by the EMC regulations, i.e. according to European CISPR 22 standard conducted emissions limits extend from 150 kHz to 30 MHz.

B. EMC Analysis based on 3D Numerical Modeling

Nowadays, with increased computational power of personal computers, virtual prototyping based on 3D electromagnetic modeling and simulation has become the state-of-the-art for EMI/EMC design of EMI filters and power converter systems [6], [23]. The theory behind 3D electromagnetic modeling is based on numerical techniques such as Finite Element Mehod (FEM), Method of Moments (MoM), Partial Element Equivalent Circuit (PEEC) method, Boundary Element/Integral Method (BEM, BIM), etc., which is rather the focus of the Computational Electromagnetics (CEM) than the Power Electronics society [24]. However, the applicability of 3D electromagnetic modeling to EMC problems in power electronics is, as it will be shown, quite significant. Concerning accuracy, computational speed and complexity, the Partial Element Equivalent Circuit (PEEC) method can be seen as the most suitable numerical technique for solving the EMC problems for power electronics applications, which in turn can be described as circuit-field coupled problems. The 3D electromagnetic modeling approach based on the PEEC method is presented in this paper in more detail with a special attention to the modeling of EMI filter components and virtual design of EMI filters in a wide frequency range.

The proposed PEEC-based modeling approach enables the modeling of full EMI filter circuits in an efficient and accurate way including both self and mutual parasitic effects. It can provide a comprehensive EMC analysis of different EMI filter structures including the influence of various effects on EMI filter performance such as components parasitics, mutual couplings, PCB layout, component placement, grounding, and shielding. A brief introduction into the PEEC modeling methodology is presented in the following section.

C. The Partial Element Equivalent Circuit Method

The PEEC method was originally derived for the electromagnetic modeling of complex IC interconnections [25]. It is based on the discretization of electrical conductors into partial elements, i.e. inductance, capacitance, resistance, and voltage/current sources. The detailed derivation of the PEEC method is given in [26] and the basic PEEC formulas are briefly summarized in Appendix. Three dimensional representation of the current flow is defined by the PEEC volume cells, and the PEEC surface cells are used as a 2D representation of the charge over the corresponding volume cells, since the charge resides on the conductor surfaces. Namely, the current volume density distribution $\vec{J}(\vec{r},\omega)$ and the electric charge density distribution $\rho(\vec{r},\omega)$ of the conductors, are approximated by the local constant basis functions. A k-th PEEC volume cell carries a total current I_k in the defined directions $\vec{f}_{0k}$ between two PEEC nodes, e.g. P_l and P_{l+1}. The voltage drop across the k-th PEEC volume cell ΔV_k represents the difference between the potentials of l-th and $(l+1)$-th PEEC nodes, $\Delta V_k = V_l - V_{l+1}$. The charges of the PEEC surface cells represent the sources of the PEEC node potentials. In this paper the PEEC discretization, i.e. PEEC meshing, is illustrated in Fig. 1 on the example of a PCB layout to give a basic understanding of the PEEC modeling methodology.

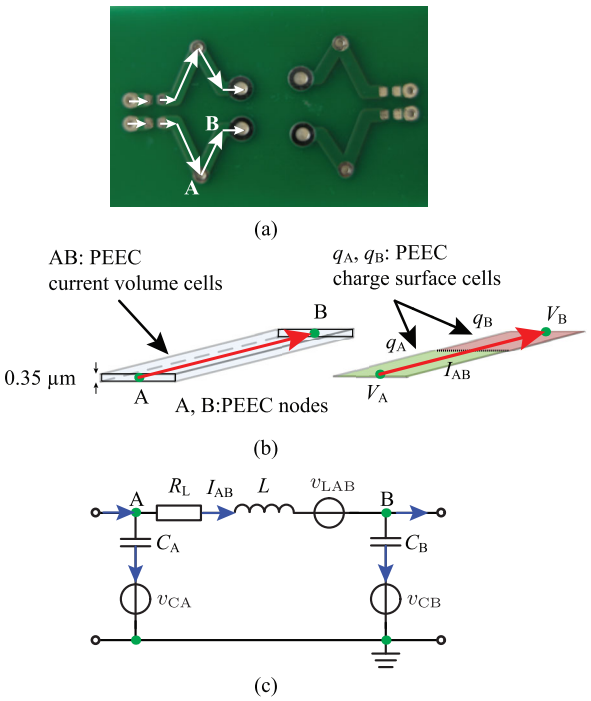

Fig. 1. PEEC modeling of a PCB layout: a) photo of a PCB layout, b) PEEC model of a PCB track, and c) PEEC equivalent circuit of the PCB track.

Starting from the real 3D geometry, the PEEC partial elements (R_L, L, C, V_L, V_C) are first extracted by means of a filament mesh [27], then the PEEC equivalent circuit can be derived from Kirchhoff's current and voltage laws, and finally solved for the unknown voltages and currents, [V, I], cf. Fig. 1, I_AB, V_A, V_B. The voltage sources V_L and V_C include mutual inductive couplings between PEEC volume cells and mutual capacitive couplings between PEEC surface cells. The PEEC equivalent circuits can be easily coupled to any circuit simulator such as e.g. SPICE or GeckoCIRCUITS [28] and solved both in the time and frequency domain. The PEEC system matrix given by (1) can be also directly calculated for the unknown currents and/or voltages in a standalone solver.

$$\begin{bmatrix} \mathbf{A} & -(\mathbf{R}+j\omega\mathbf{L}) \\ (j\omega\mathbf{P}^{-1}+\mathbf{Y}_\mathrm{L}) & \mathbf{A}^\mathrm{T} \end{bmatrix} \begin{bmatrix} \mathbf{V} \\ \mathbf{I} \end{bmatrix} = \begin{bmatrix} \mathbf{V}_\mathrm{S} \\ \mathbf{I}_\mathrm{S} \end{bmatrix} \qquad (1)$$

The matrix $\mathbf{A}$ is the connectivity matrix defining the connection between PEEC partial elements, $\mathbf{R}$ is the resistance diagonal matrix, $\mathbf{L}$ is the inductance matrix consisting of the self (L_{ii}) and mutual (L_{ij}) inductances between PEEC volume cells, $\mathbf{C}$= $\mathbf{P}^{-1}$ is the capacitance (potential) matrix defining

the self (P_{ii}) and mutual (P_{ij}) potentials of PEEC surface cells, $\mathbf{Y}_\mathrm{L}$ is the admittance matrix consisting of matrix stamps of additional circuit elements connected between PEEC nodes, and $\mathbf{I}_\mathrm{S}$ and $\mathbf{V}_\mathrm{S}$ are current and voltage sources for modeled excitations [26], [27]. Optionally, magnetic and electric field strengths can be calculated in a post-processing step via the current distribution $\mathbf{I}$, and the voltage potentials $\mathbf{V}$.

In comparison to the Finite Element Method (FEM), the discretization of the surrounding air volume is not required and only the meshing of conducting, dielectric, and magnetic volumes has to be performed [29]. Accordingly, the PEEC method turns out to be a fast and accurate modeling approach for circuit-field coupled problems such as PCB tracks, EMI filters, power converter systems, etc.

The main difficulty of the PEEC method is modeling in the presence of magnetic materials. Concerning power electronics applications, this difficulty reflects to the PEEC-based modeling of magnetic components like inductors and transformers utilizing magnetic core material. The PEEC-based modeling of nonlinearity, anisotropy, and other magnetic properties is not straightforward and is not performed in practice. As a result, exact 3D PEEC-based models of magnetic components are not possible and the finite element analysis is typically applied for this class of problems.

PEEC-based modeling of practical inductors was discussed in [10], [30]–[33]. The authors developed PEEC models of toroidal inductors under the assumptions that the direction of the stray field produced by an inductor is not influenced by its constitutive ferromagnetic magnetic material. This method was then applied to the modeling of single-phase common-mode inductors used in EMI input filters where the leakage field is generated by DM currents. The near field coupling between magnetic components and the stray magnetic field lines of toroidal inductors used in EMI filters were investigated also in [34] following a similar PEEC modeling methodology. However the direction of the field lines was measured and simulated only for inductors with uniform winding arrangments. In particular, a clear understanding of the stray field generated by toroidal inductors having an arbitrary winding arrangment has been missing and the corresponding PEEC models have been only approximately developed, as it was shown in [10], [30]–[33].

The magnetic characteristics of the cores used in practice can be described by means of the relative (complex) permeability coefficient which allows the homogenization and linearization of the core properties and thus, the application of the linear modeling approach such as the PEEC-method. Accordingly, an extended PEEC method was developed and introduced in [13], [14] enabling the modeling of the magnetic components taking into account both the internal and external properties, i.e. the magnetic field inside and outside of the magnetic core, as it was fully verified in [35]. The modeling principles are explained in the next subsection.

D. The PEEC-Boundary Integral Method

As it is already emphasized, an extension of the PEEC method was required in order to calculate and to correctly model the electromagnetic influence of magnetic components. Specifically, it was shown in [13] that a magnetic core could be modeled as a homogenous and linear material defined by the relative (complex) permeability coefficient μ_r. Since the practical design of inductors and transformers is based on frequency dependent permeability curves, $\mu_\mathrm{r}(f)$, given by manufacturers or measured, the homogenization assumption is fully justified for power electronics applications (as long as core is not operated in highly non-linear range), which simplifies the PEEC-based modeling of magnetic components in the frequency domain.

According to electromagnetic theory, the influence of a magnetic core can be modeled by replacing the core with a fictitious distribution of magnetic volume $\vec{J}_\mathrm{M}$ and surface $\vec{K}_\mathrm{M}$ currents. For a linear case, it is shown that the magnetic volume currents do not have to be directly calculated and only the surface of the magnetic core has to be taken into account. This implies the extension of the PEEC EFIE (A.1) with the term $j\omega\vec{A}_\mathrm{M}$, where $\vec{A}_\mathrm{M}$ represents the magnetic vector potential generated by the magnetic surface currents $\vec{K}_\mathrm{M}$. Following the PEEC modeling methodology, the magnetic surface is discretized into N_M surface panels, so that the magnetic surface current distribution is represented with N_M current filaments. The inductive coupling between the magnetic surface currents and the winding currents can be expressed via the matrix $\mathbf{L}_\mathrm{M}$. The $\mathbf{L}_\mathrm{M}$ elements are the mutual inductances between the magnetic current and electric current filaments calculated using the formulas from [27]. Furthermore, the coupling between the fictitious magnetic currents and the electric currents is derived from the boundary condition for the tangential component of magnetic field lines $\vec{H}_\mathrm{t}$, i.e. $\mathbf{H}_\mathrm{t}$-boundary conditions. For each surface panel, the boundary condition equation can be calculated for its central point C_k, i.e. collacoation method [36], cf. Fig. 2. As it was described in [13], [14], [35], the boundary condition equation can be written in a matrix form by means of $\boldsymbol{\alpha}_\mathrm{MM}$ and $\boldsymbol{\lambda}_\mathrm{MI}$ matrices. This leads to a new PEEC-Boundary Integral Method (PEEC-BIM) and to introducing the magnetic surface currents as additional unknowns. Consequently, the PEEC-BIM system matrix in the presence of magnetic cores has to be extended by additional columns and rows, i.e. $\boldsymbol{\alpha}_\mathrm{MM}$, $\boldsymbol{\lambda}_\mathrm{MI}$ and $\mathbf{L}_\mathrm{M}$ matrices, in order to calculate the unknown $\vec{K}_\mathrm{M}$ current distribution (2).

$$\mathbf{M}_\mathrm{sys} = \begin{bmatrix} \mathbf{A} & -(\mathbf{R}+j\omega\mathbf{L}) & -j\omega\mathbf{L}_\mathrm{M} \\ (j\omega\mathbf{P}^{-1}+\mathbf{Y}_\mathrm{L}) & \mathbf{A}^\mathrm{T} & \mathbf{0} \\ \mathbf{0} & \boldsymbol{\lambda}_\mathrm{MI} & \boldsymbol{\alpha}_\mathrm{MM} \end{bmatrix} \tag{2a}$$

$$\mathbf{M}_{sys} \begin{bmatrix} \mathbf{V} \\ \mathbf{I} \\ \mathbf{K}_\mathrm{M} \end{bmatrix} = \begin{bmatrix} \mathbf{V}_\mathrm{S} \\ \mathbf{I}_\mathrm{S} \\ \mathbf{0} \end{bmatrix} \tag{2b}$$

The $\mathbf{L}_\mathrm{M}$ matrix includes the mutual inductances between PEEC volume cells, e.g. electrical conductors, and the magnetic currents $\vec{K}_M$. The elements of $\boldsymbol{\alpha}_\mathrm{MM}$ and $\boldsymbol{\lambda}_\mathrm{MI}$ matrices are calculated via the $\mathbf{H}_\mathrm{t}$-boundary conditions that have to be satisfied at the points of the magnetic core surface, i.e. material interface. The PEEC-BIM modeling principles are illustrated on the example of a toroidal inductor in Fig. 2. The PEEC-

BIM method is implemented and verified for the toroidal core shape which is typically used for EMI input filter inductors.

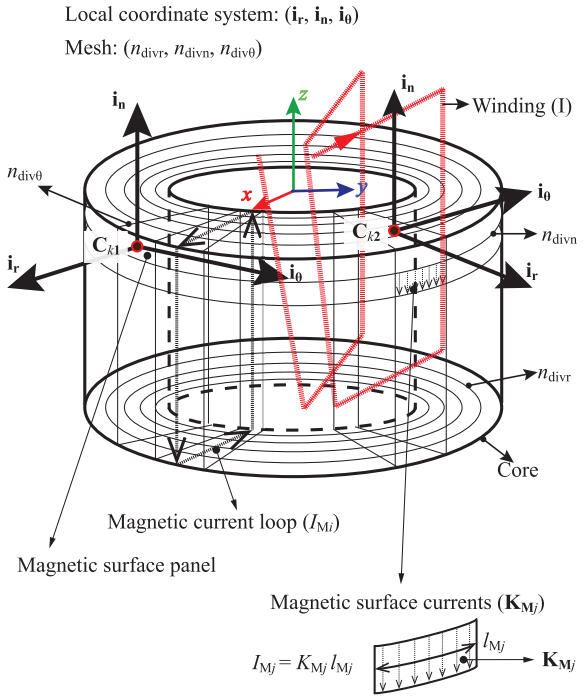

Fig. 2. PEEC-BIM modeling of a magnetic inductor with toroidal core. The mesh of the core surface in the cylindrical coordinate system ($\vec{i}_r$, $\vec{i}_\theta$, $\vec{i}_n$) is represented by $N_{\mathrm{M}} = n_{\mathrm{div}\theta} \cdot (2n_{\mathrm{divr}} + 2n_{\mathrm{divn}})$ magnetic surface panels with the central points C_k. The turns carrying the electric currents I are modeled by the PEEC cells distributed around the core in the same way as the actual winding (red-dotted line). The magnetic surface currents $\mathbf{K}_{\mathrm{M}}$ are modeled by the current filaments existing over the magnetic panels. By merging the magnetic panels at the same angles θ_k, $n_{\mathrm{div}\theta}$ magnetic current loops carrying the total magnetic current $I_{\mathrm{M}k}$ can be defined.

The proposed PEEC-BIM modeling approach has been implemented in a 3D EMC simulation tool, GeckoEMC. In the next section, it is shown that the EMC modeling environment, GeckoEMC can provide detailed EMC analysis of EMI filter components.

III. PEEC-based Modeling of EMI Filter Components

The detailed description of the PEEC-BIM models of EMI filter components is given in [11], [12]. The PEEC-BIM models of the EMI filter inductors and capacitors are defined by the same geometrical properties as the actual components. On the other hand, it can be said that material properties represent more critical input, as additional measurements are required, i.e. permeability measurements in the case of inductors and impedance measurements for fitting the properties of the PEEC cell used to model X/Y EMI filter capacitors. As it was shown in [11], [12], solid wires and PCB tracks are modeled by means of cylindrical and rectangular PEEC cells.

The corresponding PEEC-based models are used to simulate self- and mutual-parasitic effects and also to distinguish and assess the influence of these effects on the HF performance of the component itself and of the overall EMI filter. Moreover, it will be shown in this paper that the parasitic cancellation techniques proposed in literature can be modeled by means of the developed 3D EMC tool. In this way, the effects of these techniques on the overall EMI filter attenuation characteristics can be evaluated for different EMI filter layouts prior to building hardware prototypes.

A. PEEC-based Modeling of PCB Layout

The best way to explain the advantage that the PEEC method has over the well-known Finite Element analysis is the example of conductors with longitudinal size several orders higher than the other two dimensions, i.e. 0.35 µm, thick PCB tracks which are several centimeters long. In that case, a very fine discretization of the conductors and also the air around the conductors is required in the FE modeling approach that implies much longer simulation time compared to the corresponding PEEC-based modeling. An example of a L-shaped PCB track with a copper layer manufactured at the bottom side of the PCB is shown in Fig. 3. The top layer L-shaped PCB track is connected to the bottom copper layer forming a conductive path between the input $\mathrm{A_{IN}}$ and output $\mathrm{A_{OUT}}$ ports. The PEEC modeling of the L-shaped conductors was verified by the impedance measurements performed by an OMICRON Bode100 vector network analyzer operating in the frequency range from 10 Hz to 40 MHz [37]. Good matching between the simulation and the measurements is achieved in the whole frequency range, cf. Fig. 4. The PEEC simulation time is of the order of tens of seconds.

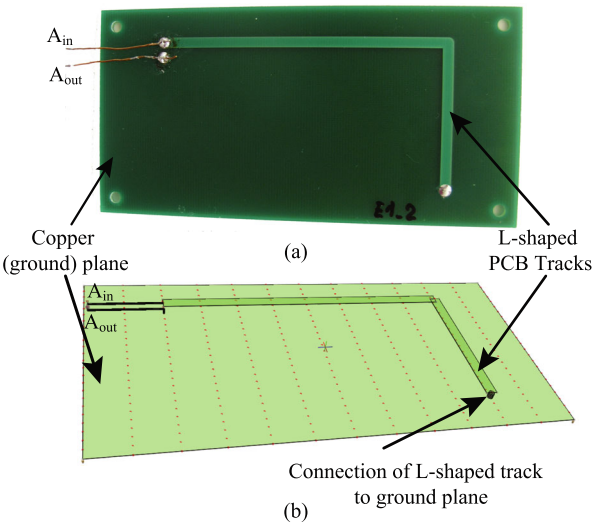

Fig. 3. A L-shaped PCB loop: (a) photo of the PCB and (b) GeckoEMC model.

B. PEEC-based Modeling of EMI Filter Capacitors

The HF equivalent circuit of EMI filter capacitors can be represented by the equivalent series inductance ESL and the equivalent series resistance ESR. The HF parasitic effects of a capacitor are determined mainly by the ESL and ESR which characterize the current path between the capacitor connectors. Accordingly, a X/Y EMI filter capacitor is modeled as a

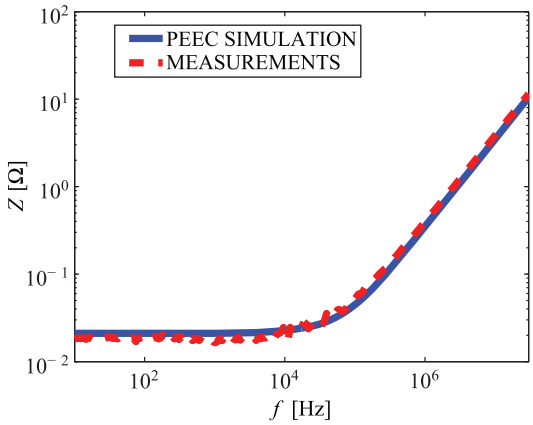

Fig. 4. Comparison between the PEEC simulation and the impedance measurements of the L-shaped PCB loop shown in Fig. 3.

rectangular PEEC cell with the same geometrical dimensions as the real capacitor [11]. It is shown that the complicated internal structure of X/Y film capacitors can be represented as a homogeneous structure with an unknown conductivity σ. The length of the capacitor connectors (len_c) and the value of σ are fitted so that the simulated and the measured total impedance of the capacitor, Z_C, match. Namely, the conductivity σ is calculated to achieve the same ESR, and the length of the connectors len_c is determined to achieve the same ESL, in the PEEC model as in the Z_C measurements. The PEEC-BIM model of EMI filter capacitors can correctly model both, the capacitor impedance and mutual coupling effects as it was shown in [11], [12]. The PEEC-BIM model of EMI filter capacitors is verified by measuring the mutual coupling between two capacitor loops, cf. Fig. 5. The mutual coupling depends on the distance d and on the current path through the capacitors. The EPCOS X2 B32924 $C = 1\,\mu\text{F}/305\,\text{V}$ capacitors are used for the verification.

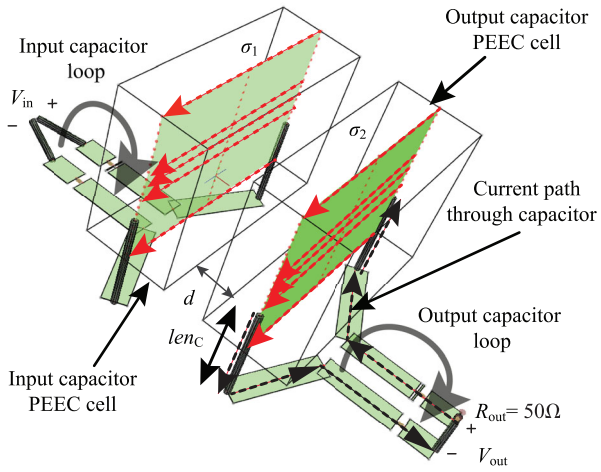

Fig. 5. GeckoEMC PEEC model of two capacitor loops.

In the next step, a cancellation loop is added to the output capacitor as shown in Fig. 6 to investigate the cancellation of the mutual coupling between two capacitors proposed in [20]. Good agreement between the PEEC simulation and the measurements of transfer function from the input to the output capacitor loop is shown in Fig. 7. The transfer function measurements were performed by an OMICRON Bode100 vector network analyzer. The results are presented from 100 kHz up to 30 MHz as the measured transfer function reached the signal-to-noise resolution limit of the measurement equipment for the lower frequencies. According to the measurements and the PEEC-BIM simulation results, cf. Fig. 7, the induced voltage in the output capacitor loop is lower in the case of the output capacitor with the cancellation turn L_M, implying that the mutual coupling between two capacitor loops is reduced for approximately 8 dB with the integration of L_M.

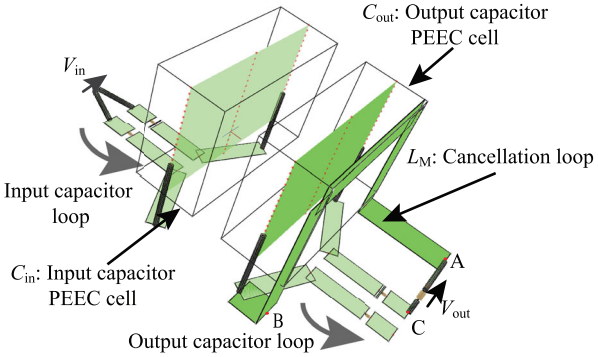

Fig. 6. GeckoEMC PEEC-model of two capacitor loops with a cancellation loop [20].

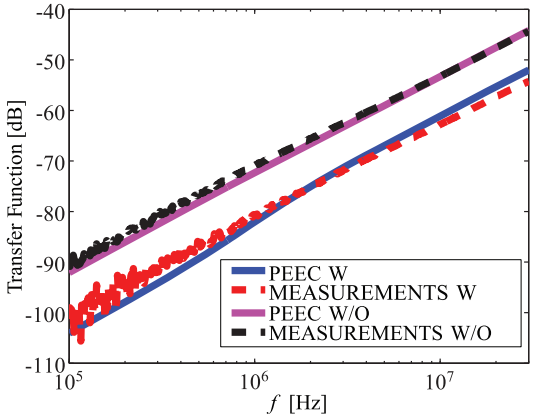

Fig. 7. Comparison between the PEEC simulation and the measurements of the transfer gain between the input and output capacitor loops with (W) and without (W/O) a cancellation loop, cf. Fig. 6.

In the next step, the ESL-parasitic cancellation technique for two parallel capacitors described in [19], [21] is analyzed in order to demonstrate the capabilities of the developed PEEC-BIM method. The equivalent circuit, the corresponding PCB layout, and the PEEC-BIM model are shown in Fig. 8. The cancellation of the parasitics of the parallel capacitors is achieved by adding the inductors $L = ESL$ in series to the signal path; so, the mutual coupling introduced by these inductors reduces the total ESL of the capacitors, cf. Fig. 8.

The inductors L are implemented using two one-turn PCB windings. Good matching between the measurements and the PEEC-BIM simulation of the transfer gain of two parallel capacitors is presented in Fig. 9. The transfer gains with and without the ESL-parasitic cancellation are shown together in Fig. 9 for comparison. The experimental results verify the improvement of the transfer gain, ΔAtt, resulting from employing the ESL-parasitic cancellation windings. However, the ESL cancellation technique should be carefully used in EMI filters, as the HF performance of EMI filters can be additionally degraded due to the mutual coupling between the cancellation loops and the other filter components.

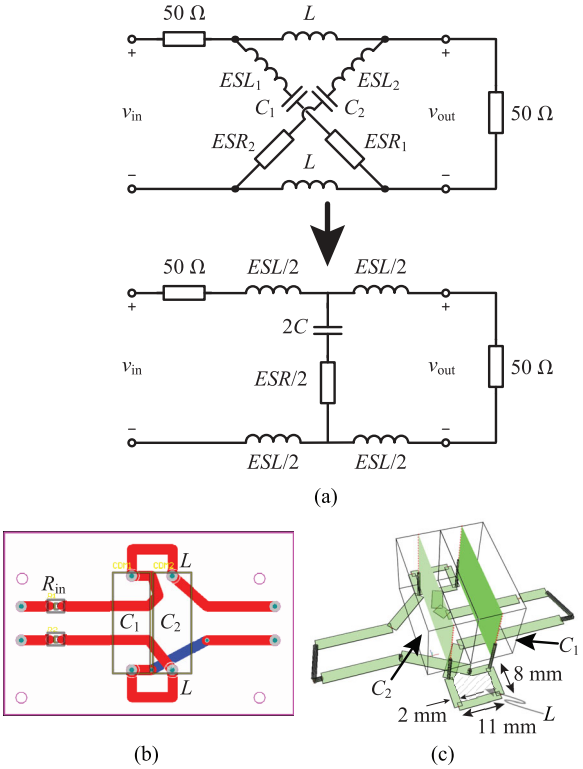

Fig. 8. ESL-parasitic cancellation technique for two parallel capacitors: (a) equivalent network circuit, (b) PCB layout, and (c) GeckoEMC PEEC model.

PEEC-BIM modeling represents a useful tool to find an optimal PCB layout and to assess the effects of different parasitic cancellation techniques.

C. PEEC-based Modeling of EMI Filter Inductors

The electromagnetic properties of the magnetic core are modeled via the coupling of two numerical techniques: the PEEC method and the Boundary Integral Method (BIM). Concerning the implementation of the PEEC-BIM approach, the main problems originate from the discretization of the core surface into a set of N_{M} panels carrying the unknown surface current density $\vec{K}_{\mathrm{Mj}}$ ($j = 1 \ldots N_{\mathrm{M}}$) and from the singularity calculation occurring in the BIM equations, i.e. the calculation of the diagonal elements of $\boldsymbol{\alpha}_{\mathrm{MM}}$ matrix [14], [35]. For this reason, every core-shape requires special modeling attention. The first modeling task concerns inductors built with

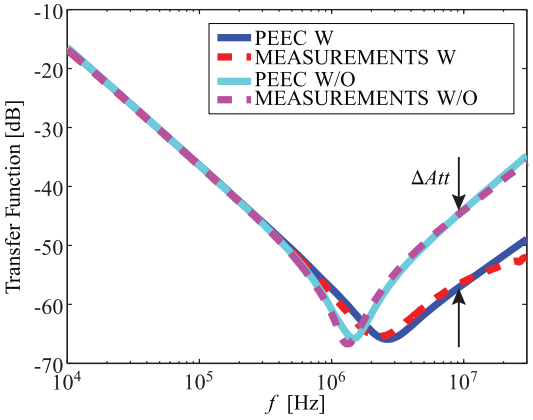

Fig. 9. Comparison between the PEEC simulation and the measurements of the transfer gain of two parallel capacitors with (W) and without (W/O) ESL-cancellation.

TABLE I
INDUCTOR SPECIFICATIONS.

	Manufacture/Material/Size	Winding	Wire
a	Vacuumschmelze/nanocrystaline VITROPERM 500F/W380 [38]	single-phase CM 2×20	AWG20
b	Vacuumschmelze/nanocrystaline VITROPERM 500F/W523	single-phase CM 2×20	AWG20
c	Magnetics/HighFlux/stacked two 58204A2 [39]	uniform DM 1 × 32	AWG20
d	Magnetics/MPP/55203A2	uniform DM 1 × 32	AWG26
e	Magnetics/KoolMμ/77935A7	uniform DM 1 × 42	AWG26
f	Micrometals/-26/T132 [40]	uniform DM 1 × 38	AWG26
g	EPCOS/Ferrite T38/R32 [41]	half-uniform 1 × 20	AWG15

toroidal cores typically used in EMI input filters. For a toroidal geometry, as shown in Fig. 2, the magnetic surface currents can be described in the cylindrical coordinate system as

$$\vec{K}_{\mathrm{M}j} = K_{\mathrm{M}\theta\mathrm{j}}\vec{i}_{\theta} + K_{\mathrm{Mr(n)}j}\vec{i}_{\mathrm{r(n)}}. \tag{3}$$

The discretization is defined in the local coordinate system ($\vec{i}_{\mathrm{r}}$, $\vec{i}_{\mathrm{n}}$, $\vec{i}_{\theta}$) by three discretization numbers (n_{divr}, n_{divn}, $n_{\mathrm{div}\theta}$) so that total number of magnetic panels is $N_{\mathrm{M}} = n_{\mathrm{div}\theta}\cdot(2n_{\mathrm{divr}}+2n_{\mathrm{divn}})$. As it was shown by the measurements, the distribution of the magnetic surface currents can be further simplified by the magnetic currents forming loops around the core circumference. Namely, the magnetic panels at the angle θ, cf. Fig. 2, can be merged into a magnetic current loop $I_{\mathrm{M}\theta j}$, $j = 1 \ldots n_{\mathrm{div}\theta}$. Therefore, in the presence of a magnetic core, the number of additional unknowns is only $n_{\mathrm{div}\theta}$, instead of N_{M}.

To verify the PEEC-BIM model of EMI input filter inductors, single-phase Common (CM) and Differential (DM) mode inductors with different winding arrangements and different core materials were investigated. A summary of the cores used for the verification of the developed PEEC-BIM model is given in Table I.

In the previous work [42], modeling of the HF response of an inductor was performed by means of a complicated RLC network, where the analytical formulas were used to

approximate the calculation of the distributed *R*, *L* and *C* parameters. In PEEC-BIM modeling of EMI filter inductors, besides the geometry parameters, the input material data are the complex permeability curves, $\underline{\mu_\mathrm{r}}\,(f) = \mu_\mathrm{r}{}'(f) - j\mu_\mathrm{r}{}''(f)$, that are measured using inductors with a lower number of turns. Accordingly, the magnetic properties are modeled by the real part of the complex permeability $\mu_\mathrm{r}{}'(f)$, while the (small signal) core losses are included via the imaginary part, $\mu_\mathrm{r}{}''(f)$. With increasing frequency and also with increasing flux density, an inductor loses its magnetic properties and the parasitic capacitance *EPC* significantly affects the frequency response of the inductor. Therefore, the parasitic capacitance *EPC* has to be modeled in order to correctly predict the HF behavior of an inductor. The single-phase DM and CM winding configuration were considered with a lower and higher number of turns to investigate the parasitic capacitive effects of EMI filter inductors, cf. Table I.

As it is well known from literature, the parasitic capacitive effects include the turn-to-turn $C_{\mathrm{t-t}}$ and turn-to-core $C_{\mathrm{t-c}}$ capacitances which cannot be distinguished easily. A way to decrease this capacitive effect is to avoid multi-layer windings, so that the turn-to-turn capacitance between the layers is eliminated. Usually, the calculation of the total winding capacitance is performed via an analytical approach described in [43]–[45]. However, the prediction of the total capacitance as described in [43] leads to an over-estimated capacitance value as it relies on some geometrical and mathematical approximations [7]. In the PEEC-BIM model, the capacitive effect is included by the **P**-matrix, cf. (2), which takes into account the turn-to-turn capacitance $C_{\mathrm{t-t}}$ of both single- and multi-layer windings and the self-capacitances. However, in literature [34], [42], [46] and also in the impedance measurement results, it is observed that the turn-to-core capacitance $C_{\mathrm{t-c}}$ can significantly increase the total winding capacitance. Therefore, it has to be taken into account. Additional C-matrices, $\mathbf{C}_{\mathrm{MI}}$, $\mathbf{C}_{\mathrm{IM}}$, and $\mathbf{C}_{\mathrm{MM}}$, modeling the turn-to-core capacitive coupling, are added into the PEEC-BIM system matrix, cf. (4), in order to correctly model the parasitics of the inductor in the HF range.

$$\mathbf{C}_{\mathrm{t-c}} = \begin{bmatrix} \mathbf{P}^{-1} & -\epsilon\mathbf{C}_{\mathrm{IM}} \\ -\mathbf{C}_{\mathrm{MI}} & -\mathbf{C}_{\mathrm{MM}} \end{bmatrix} \tag{4}$$

The elements of the matrices are derived from the capacitive coupling between the magnetic surface panels and the winding using the same approach as for the calculation of **P**-matrix elements [27], [47]. As a result, new unknowns are the potentials of the N_{M} magnetic surface panels, carrying free electrical charges. Furthermore, a coefficient ϵ is used to fit the measurement results as $C_{\mathrm{t-c}}$ depends on the distance between the core and the winding which varies along the core circumference and also on the actual core packaging properties, which are hard to be determined. The turn-to-core capacitances $\mathbf{C}_{\mathrm{t-c}}$ and the self-capacitances recalculated from the diagonal **P**-matrix elements, P_{ii} (1), take into account the effect of the displacement currents, which in turn have a significant influence on the near field coupling between the inductor and the other components at higher frequencies [34].

The comparison of the PEEC-BIM simulation and impedance measurements of the inductors specified in Table I is presented in Fig. 10. The inductors are built with a higher number of turns closely wound around the core. In the first approach, only the turn-to-turn capacitance is taken into account. As it is shown in Fig. 10, using the modified **C**-matrix, better matching between the PEEC-BIM simulation and the measurements is achieved in the HF range.

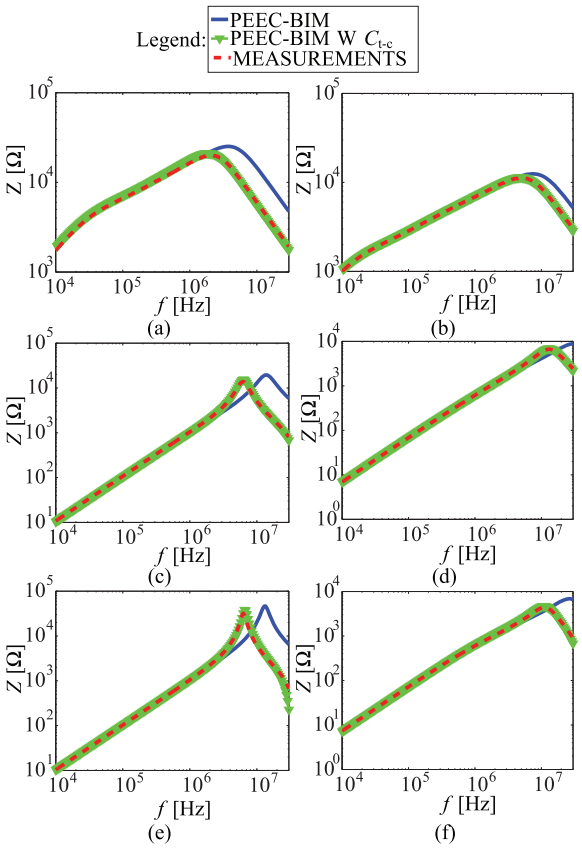

Fig. 10. Comparison between the PEEC simulation and the impedance measurements of the inductors (a) - (f) specified in Table I with modeling $C_{\mathrm{t-c}}$, i.e. PEEC simulation W $C_{\mathrm{t-c}}$.

Exemplarily, the inductor (c) is then used to investigate the turn-to-core capacitive in more detail. The permeability curves are extracted from the impedance measurements of a 6-turn uniform winding (wire diameter $1.4\mathrm{mm}$) built on a single core Magnetics HighFlux 58204 for the frequencies up to $110\mathrm{MHz}$. The impedance measurements were performed using Agilent 4294A impedance analyzer operating in the frequency range from $40\,\mathrm{Hz}$ up to $110\,\mathrm{MHz}$. The measured impedance and the extracted permeability curves are given in Fig. 11.

As it can be observed, the inductor losses its magnetic properties in the frequency range above $f_{\mathrm{C}} = 20\,\mathrm{MHz}$, which means that the inductance L_{DM} decreases and the equivalent parallel capacitance EPC starts to have a significant effect. Namely, the calculated permeability curves do not carry only the information about magnetic properties at higher frequencies and thus they do not represent fully accurate input parameters in the whole frequency range. The PEEC-BIM modeling of the 32-turns winding inductor built on two stacked HighFlux 58204 cores was then performed with and

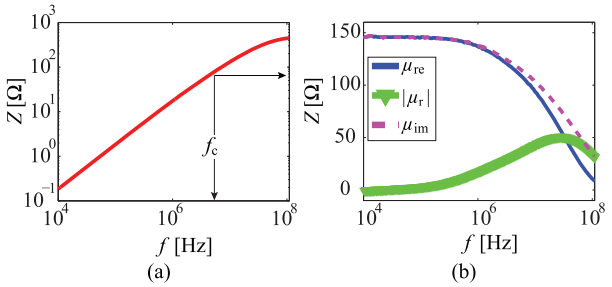

Fig. 11. Permeability data used to model the inductor (c) specified in Table I: (a) the measured impedance of a 6-turn uniform winding (wire diameter 1.4 mm) built on a single core Magnetics HighFlux 58204 and (b) the extracted permeability curves.

without using modified matrix $\mathbf{C}_{\mathrm{mod}}$. The two stacked cores are modeled as a single core with the cross section twice the cross section of HighFlux 58204 core. The impedance measurements and the corresponding PEEC-BIM calculated impedance are shown in Fig. 12 on the same plot.

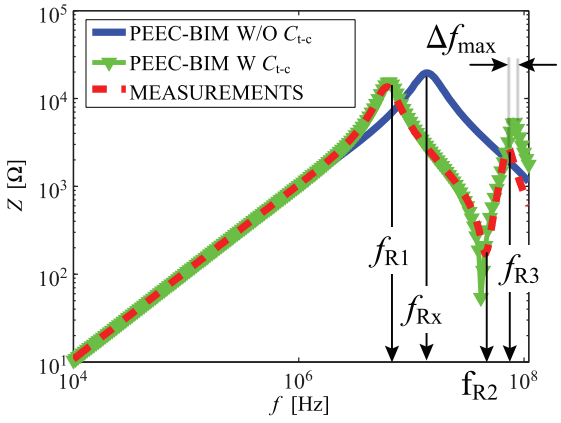

Fig. 12. Comparison between the PEEC-BIM simulation and the impedance measurements of the inductor (c) specified in Table I without and with the inclusion of the turn-to-core capacitance modeling (ϵ = 1) in the frequency range from 10 kHz up to 110 MHz.

Three resonances can be observed in the measured frequency response of the inductor: $f_{\mathrm{R}_1} = 6.4$ MHz, $f_{\mathrm{R}_2} = 47$ MHz and $f_{\mathrm{R}_3} = 72$ MHz. The PEEC-BIM modeling using only the $\mathbf{P}$ matrix returns only one resonant frequency at $f_{\mathrm{R}_x} = 13.5$ MHz but all three resonances can be observed in the calculated frequency response when the modified $\mathbf{C}_{\mathrm{mod}}$ matrix is employed. Accordingly, the presented comparison points out to the effect of the turn-to-core capacitance. A small mismatch above 20 MHz of less than $\Delta f_{\max} = 6$ MHz frequency shift can be explained by the inaccurate input parameters, i.e. the permeability curves shown in Fig. 11.

The modeling of ferrite cores requires more detailed analysis due to the dielectric core properties. Specifically, as ferrites are characterized by higher relative permittivity $\epsilon_{\mathrm{r}} = \epsilon_{\mathrm{r}}{}' - j\epsilon_{\mathrm{r}}{}''$, the manufacturers measure permeability characteristics on small ring cores, e.g. R10, to avoid dimensional effects [48]. The PEEC-BIM simulation and the impedance measurement results of the inductor built on EPCOS ferrite T38 R34 core are presented in Fig. 13(b). The simulation results comply with the measurements in the frequency range up to f_1. It can be seen from the permeability measurements performed on the inductor with only three turns cf. Fig. 13(a), that the real permeability decreases and becomes negative from $f_1 \approx 2$ MHz and the total permeability approaches zero above 10 MHz. This implies that the inductor with only three turns becomes capacitive in the frequency range from $f_1 \approx 2$ MHz which can be ascribed to high core relative permittivity, $\epsilon_{\mathrm{r}} \approx 2 \cdot 10^5$ [49]. As the manufacturer datasheets also provide the permeability curves up to a few MHz, it can be said that the PEEC-BIM simulation returns valuable results for the design and modeling of the inductors with ferrite cores.

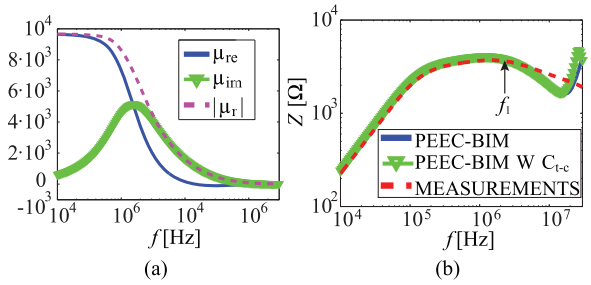

Fig. 13. The inductor (g) specified in Table I: (a) the measured permeability curves and (b) comparison between the PEEC simulation and the impedance measurements with (W) and without (W/O) $C_{\mathrm{t-c}}$.

The circuit presented in Fig. 14(a) was used to investigate the parasitic cancellation technique for the inductor winding capacitance described in [21], [50]. The actual test circuit consists of a single-phase CM inductor built on a nanocrystalline VITROPERM 500F W380 core with a (horizontal) 2×20 turns winding configuration. The PEEC-BIM model and the actual implementation of the circuit are presented in Fig. 14(b)-(c).

The two windings facilitate a high coupling coefficient so the cancellation technique can be applied. The cancellation capacitors are implemented as two SMD parallel capacitors. As the total parallel parasitic capacitance of the winding measured with the OMICRON Bode100 impedance analyzer is $EPC = 2.7$ pF, the cancellation capacitors C_{add} should be closed to $2EPC$. The transfer function measurements, $Att = 20 \cdot \log V_{\mathrm{out}}/V_{\mathrm{in}}$, are performed with and without the EPC cancellation capacitors. The turn-to-core capacitive effect, $C_{\mathrm{t-c}}$ has to be included in the PEEC-BIM model in order to achieve good matching between the measurements and the simulation results, cf. Fig. 15(a). The improvement of the inductor transfer function with EPC cancellation is presented in Fig. 15(b). A CM Y capacitor, $C_{\mathrm{add}} = 4.7$ nF, is added into the circuit to verify the influence of the EPC-cancellation on the performance of a *L-C* filter circuit. According to the results presented in Fig. 15(c), the HF performance of the observed *L-C* filter is not improved significantly using an inductor with EPC-cancellation.

The developed PEEC-BIM model of an inductor can also explain the stray field generated by EMI filter inductors [13], [35]. It was shown that the stray magnetic field lines are more pronounced in the case of non-uniform winding arrangement as it is the case with the leakage impedance of a single-phase

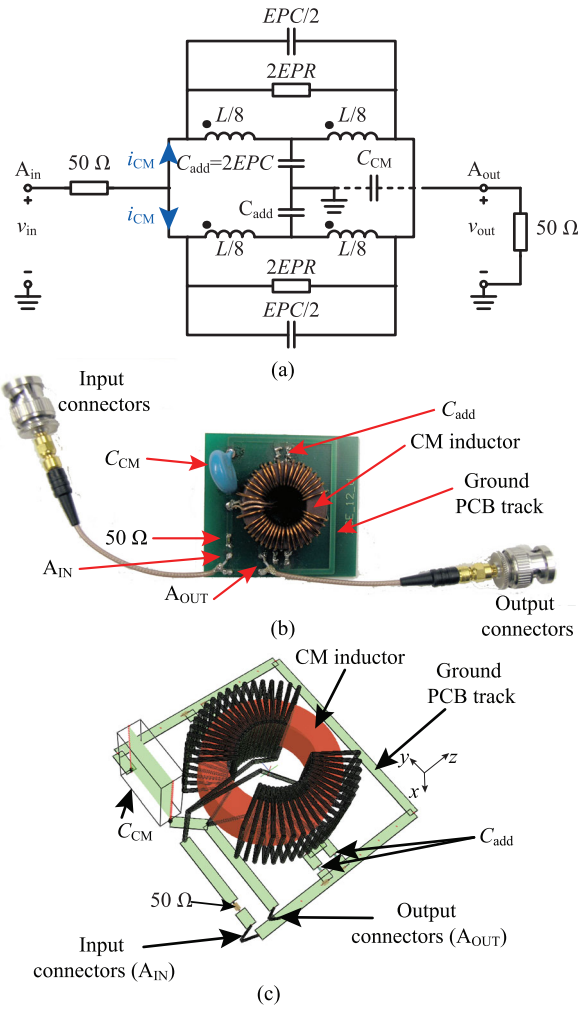

Fig. 14. *EPC* parasitic cancellation of a CM inductor: (a) equivalent network circuit, (b) photo of the actual structure, and (c) GeckoEMC model.

CM inductor, $Z_{\mathrm{CM,DM}}$. The PEEC-BIM modeling results for different cores clearly show that $Z_{\mathrm{CM,DM}}$ mainly depends on core shape and winding arrangement, and it is not affected by the capacitive coupling between the core and the winding.

IV. PEEC-based Modeling of EMI Filter Circuit

In the previous section, it is shown that the HF behavior of EMI filter components can be accurately predicted by the PEEC-BIM modeling approach. Furthermore, the 3D electromagnetic modeling allows EMC analysis of the parasitic effects within complete EMI filter circuits as it will be shown in the following on the examples of *L-C* and *C-L-C* filter structures. The transfer function measurements are performed using an OMICRON Bode100 vector network analyzer operating in the frequency range of 10 Hz to 40 MHz. The 50 Ω resistors are added to the signal path to match the 50 Ω output resistance of the measurement equipment.

A. Modeling of L-C Circuit

The GeckoEMC models and the photos of the actual *L-C* structures are shown in Fig. 16.

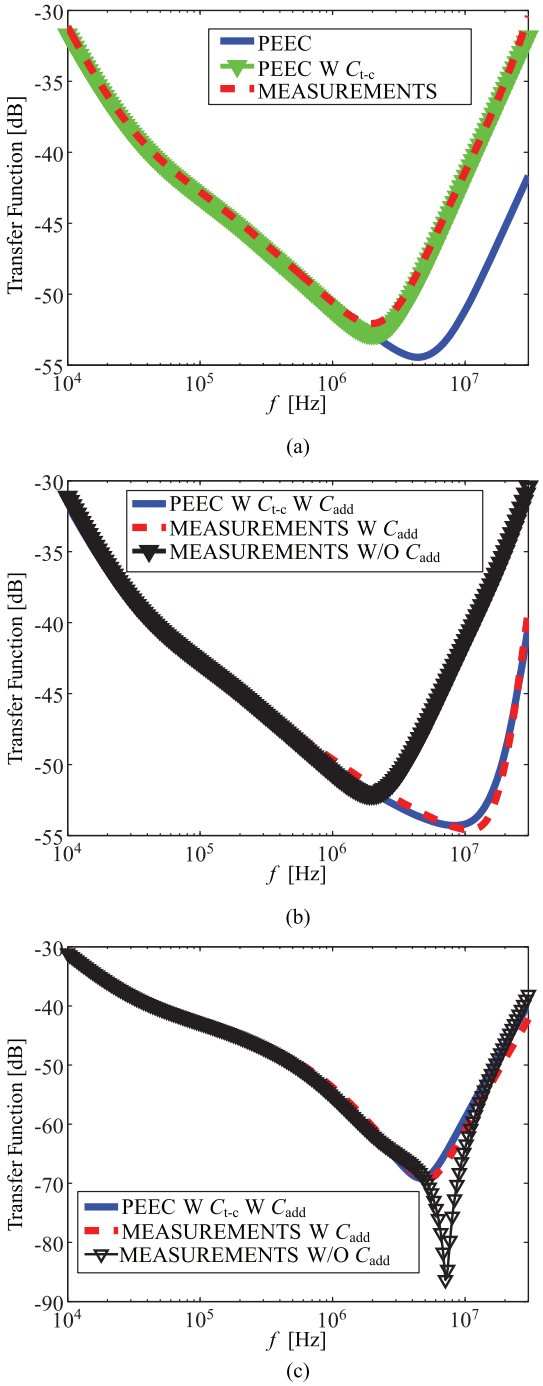

Fig. 15. Comparison between the PEEC simulation and the transfer function measurements of the circuit in Fig. 14: (a) PEEC simulation with (W) and without (W/O) $C_{\mathrm{t-c}}$, (b) PEEC simulation with $C_{\mathrm{t-c}}$, the influence of C_{add}, and (c) PEEC simulation with $C_{\mathrm{t-c}}$ the influence of both $C_{\mathrm{t-c}}$ and C_{add}.

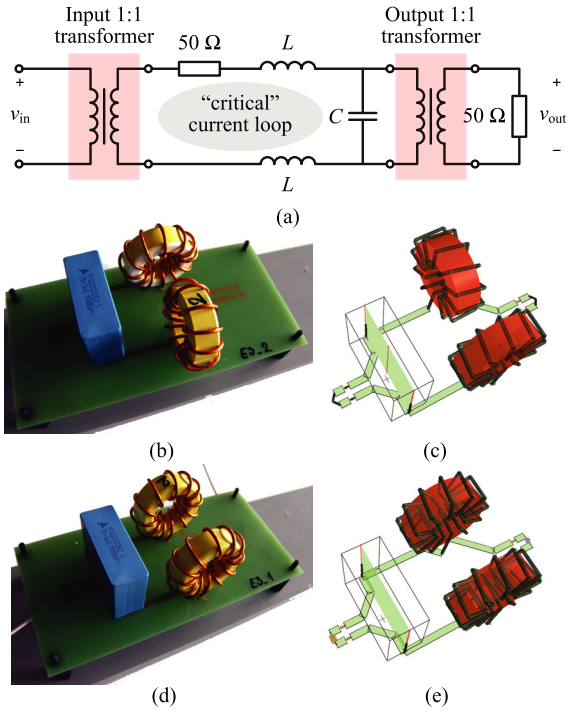

Fig. 16. $L-C$ filter modeling example: (a) equivalent network circuit; Normal position of inductors: (b) photo of the actual structure and (c) GeckoEMC model; Parallel position of inductors: (d) photo of the actual structure and (e) GeckoEMC model.

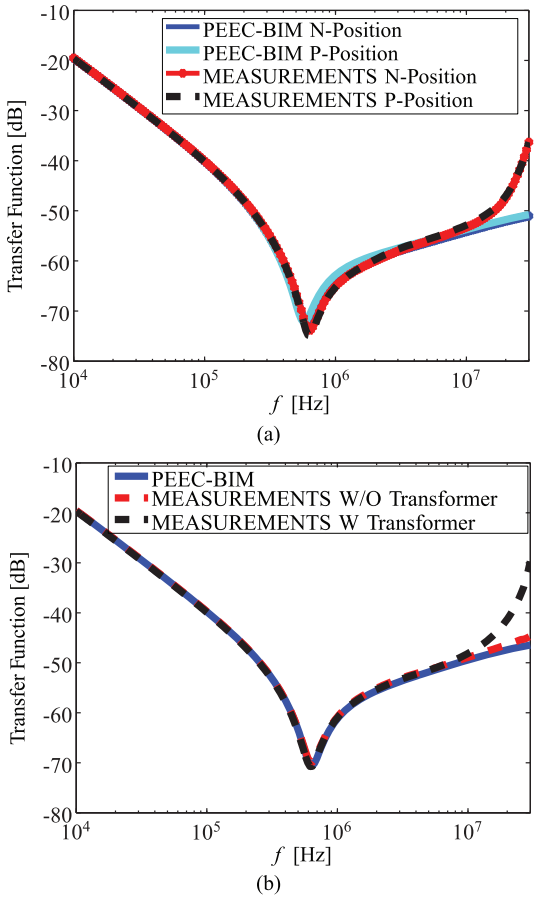

Fig. 17. Comparison between the PEEC simulation and the transfer function measurements of the L-C filters presented in Fig. 16: (a) P-Position: parallel, N-Position: normal position of two inductors and (b) with only one inductor L (W: with, W/O without 1:1 transformer).

The inductors are built on Magnetics iron powder -26 T132 cores, with 1×12 turns uniform windings and a wire diameter of 1.4 mm. The capacitor is an EPCOS X2 B32926 3.3 µF/305 V with lead spacing of 37.5 mm. Two different component arrangements are used to evaluate the dominant parasitic effects: (1) parallel and (2) normal mutual position of the two inductors. The transfer function measurements indicates that the mutual position of the inductors does not have a significant impact on the L-C filter performance in the whole frequency range. Consequently, it can be concluded that the main coupling originates from the current loop formed by the PCB tracks and the current path through the capacitor. The mismatch between the PEEC-BIM simulation and the measurements of the filter transfer function above 10 MHz, shown in Fig. 17, originates from the HF parasitics of the 1:1 transformers that have to be used to prevent short-circuiting the series impedance in the ground path across the measurement equipment [12]. The second inductor L in the ground path, cf. Fig. 16(a), is replaced by a short circuit. In this case, the measurements can be performed without the employment of the input and output isolation transformers. The comparison between the PEEC-BIM simulation and the measurements of the L-C circuit with only one inductor is presented in Fig. 17(b), showing the influence of the transformer at the input on the measurement results. The 3D EMC modeling in GeckoEMC can be performed in a step-by-step manner to investigate the coupling effect inserted by an EMI filter component.

B. Modeling of Shielding Effects in C-L-C Circuit

The examples of the C-L-C structure, shown in Fig. 18, are used to verify the influence of the mutual electromagnetic coupling between the capacitors and three shielding copper walls. The equivalent inductance of the C-L-C circuit is the leakage inductance of the single-phase CM inductor implemented with a VAC VITROPERM 500F W380 core, with a (horizontal) 2×7 winding configuration and a wire diameter of 1.4 mm. The DM capacitors are EPCOS X2 B32926 3.3 µF/305 V with a lead spacing of 37.5 mm. The PCB tracks are manufactured as the top layer and the copper (ground) plane, GP, is the bottom layer of the PCB. The shielding copper (Cu) walls of thickness 0.2 mm are inserted and soldered on the ground layer through the slots on the PCB. The distance between the copper walls and the capacitors is minimal, i.e. approximately 1 mm, so that the electromagnetic coupling effect generated by stray magnetic field lines of the input and output capacitor loops can be observed.

The simulated and the measured transfer function are presented in Fig. 19.

The influence of the mutual coupling effect inserted by the copper walls is shown by the comparison of three transfer functions: (1) without shielding walls, (2) with two vertical

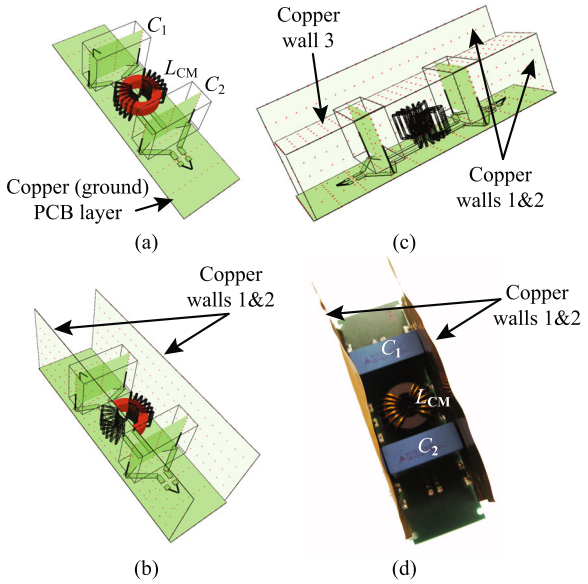

Fig. 18. The *C-L-C* filter structure: (a) without shielding walls, (b) with two vertical shielding walls, (c) with two vertical and a horizontal shielding walls, and (d) photo of the actual structure.

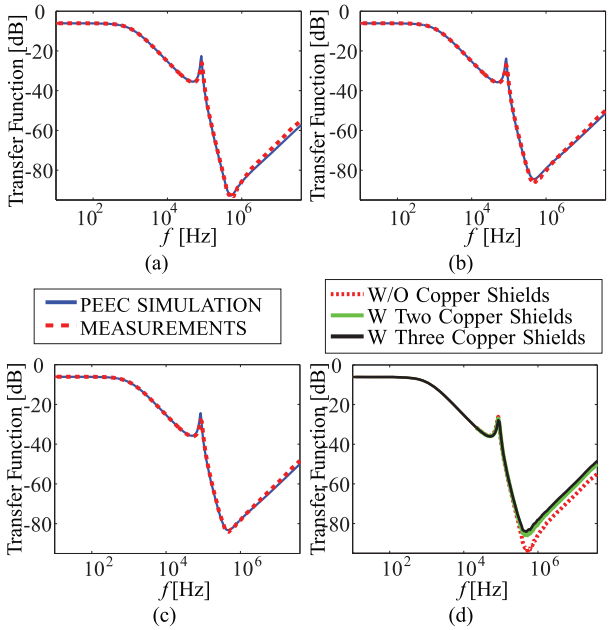

Fig. 19. Comparison between the PEEC simulation and the transfer function measurements of the *C-L-C* filter presented in Fig. 18: (a) without copper walls, (b) with two copper walls, (c) with three copper walls, and (d) the shielding effect of copper walls.

shielding walls, and (3) with three shielding walls. The presence of the copper shields decreases the attenuation in the HF range. The current paths through the capacitors together with the PCB tracks form the input and output current loops which are the sources of the stray electromagnetic field lines, which in turn induce the eddy currents within the copper walls. Furthermore, the mutual electromagnetic interaction between the copper walls and the current loops affects the filter attenuation at higher frequencies.

C. Modeling of PCB layout Effects in C-L-C Circuit

Three EMI filter structures, represented by the equivalent circuit, shown in Fig. 20(a), were modeled in the GeckoEMC simulator to verify the electromagnetic effects of the PCB layout, the copper ground plane and the distance of components on EMI filter attenuation. The first layout I exhibits a close PCB arrangement of the DM capacitors and the CM inductor cf. Fig. 20(b)-I without a copper layer. In the second layout II, the copper (ground) plane is included as bottom layer of the PCB, cf. Fig. 20(b)-II, while in the third layout III the distance between the components is increased by 10 mm keeping the copper (ground) plane the same, cf. Fig. 20(b)-III.

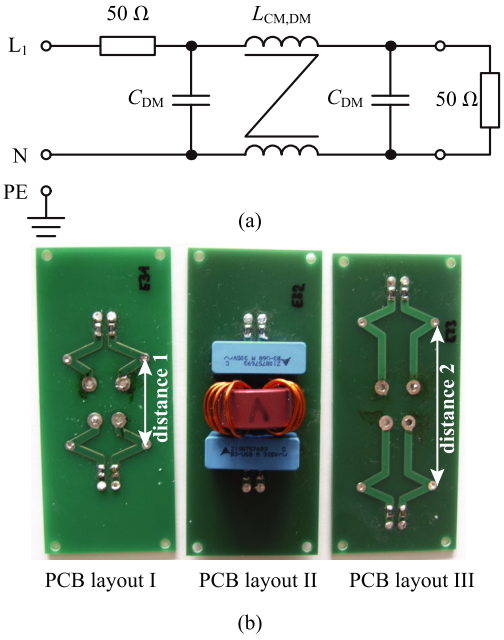

Fig. 20. *C-L-C* filter used to verify the electromagnetic effects of PCB layout, the copper ground plane, and the distance of components on EMI filter attenuation: (a) equivalent electrical circuit and (b) three (I, II, III) PCB layouts.

The equivalent DM inductance of the *C-L-C* circuit is the leakage inductance of the single phase CM inductor built on a VAC VITROPERM 500F W380 core, with a vertical 2×7 winding configuration and wire diameter of 1.4 mm. The DM capacitors are EPCOS X2 B32924 0.68 µF/305 V with lead spacing of 27.5 mm. The copper layer behaves like a floating ground in the measurements and the 1:1 input and/or output transformers are used to prevent short-circuiting the series

impedance in the ground path across the measurement equipment. Good agreement between the measurements and the PEEC-BIM simulation results of the filter transfer functions is given in Fig. 21.

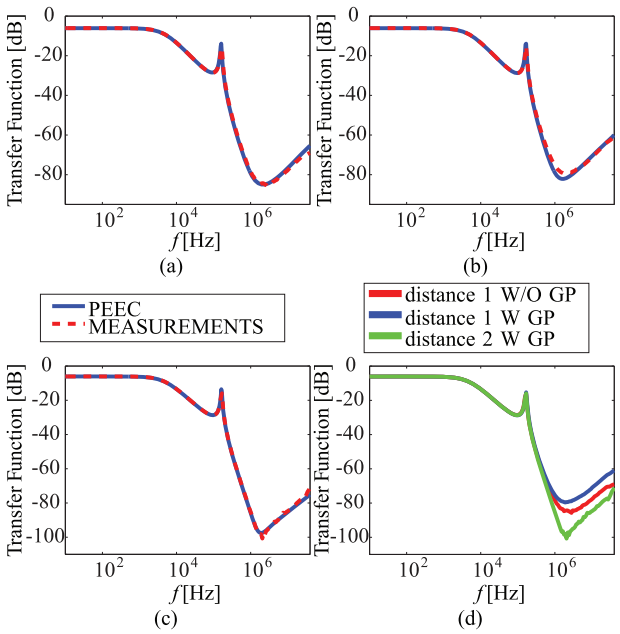

Fig. 21. Comparison between the PEEC simulation and the transfer function measurements of the *C-L-C* filter presented in Fig. 20: (a) without(W/O) copper (ground) layer, distance 1 (b) with (W) ground layer, distance 1, (c) with (W) ground layer, distance 2, and (d) PCB layout influence.

The comparison of three transfer functions can be used to explain the influence of the copper ground plane and the mutual distance of the components on the EMI filter insertion loss. Namely, the EMI filter attenuation is decreased by approximately 5 dB, due to the eddy currents induced within the conductive bottom layer of the PCB, and in turn it is improved by increasing the distance between in the components which can be explained by the reduction of the mutual parasitic coupling effect between the EM filter components and the current loops.

V. PEEC-BIM Simulation Performance

The main bottleneck of the standard PEEC method is a dense system of linear equations, which limits the maximum problem size. Different techniques have been proposed in literature to accelerate the calculation and solving of the PEEC system matrices. In addition, the computational power of today's personal computers enables the PEEC-based EMC analysis of larger structures containing over 50,000 unknown currents and voltages.

For the PEEC-BIM method, the linear system of equations is extended by the additional dense and full matrices $\mathbf{L}_{\mathrm{M}}$, $\boldsymbol{\alpha}_{\mathrm{MM}}$, and $\boldsymbol{\lambda}_{\mathrm{MI}}$ (1). Accordingly, the extension of the standard PEEC method represents a difficulty for the PEEC-based modeling of geometrically complex problems with regard to the required memory storage and the computation of inverse matrices. In the current version of the GeckoEMC simulation tool, the PEEC-BIM system equations are solved via a stand-alone direct-solver and the maximum matrix size is of the order of $10^4 \times 10^4$. In the course of future research, the implementation and efficiency of different compression techniques for the PEEC-BIM integral equations will be examined.

The meshing of the magnetic surface into N_{M} panels determines the computational complexity and accuracy of the implemented PEEC-BIM method. The simulations were performed on standard PCs with 48 GB RAM and a CPU clock frequency of 2.67 GHz. The calculation time can be separated into the pre-calculation of PEEC-BIM matrix elements and the post-calculation, e.g. the calculation of the transfer function at N_{F} points in the frequency domain.

For example, the PEEC-based modeling of the single-phase EMI filter presented in Fig. 18(b) results in a 2299×2299 square system matrix, and requires a simulation time of approximately 3 min for pre-calculation and 2 s per frequency point for post-calculation. The good matching between the measurements and the PEEC-BIM simulation results demonstrates that the PEEC discretization enables accurate 3D modeling of power electronic systems with reasonable computational effort.

VI. Conclusion

The work presented in this paper enables comprehensive electromagnetic analysis of EMI filter components and full EMI input filter circuits. The 3D electromagnetic modeling based on the PEEC modeling approach is introduced as a useful and computationaly efficient tool for prediction of the high frequency performance of EMI filter inductors, capacitors and their mutual PCB placement within actual EMI filter structures. It was shown that the PEEC-based modeling can describe self- and mutual-parasitic effects that determine the HF behavior of EMI filter components and hence also the overall EMI filter insertion loss.

The standard PEEC modeling approach was extended to the PEEC-BIM coupled method which allows the modeling of the magnetic components used in power electronic applications. Moreover, it was shown that the EMI input filter inductors built on toroidal cores can be fully described by the developed PEEC-BIM coupled method concerning both the internal and stray electromagnetic properties. Different core materials and winding arrangements were investigated. The magnetic properties and core losses are modeled by the measured complex permeability curves used as the input parameters. The winding capacitive effect is modeled by the means of a $\mathbf{C}$ matrix taking into account both the influence of turn-to-turn and turn-to-core capacitive coupling. It is shown that the turn-to-core capacitance has a significant effect in the high frequency range especially for windings with a higher number of turns. The fitting parameter ϵ can be used to model this capacitive effect which is in turn difficult to measure directly. The modeling procedure is verified by various impedance measurements.

It is demonstrated that the PCB layout and the conductive loops including the current paths through the EMI filter capacitors can have a dominant effect on EMI filter attenuation in HF range above a few MHz. As the well-known parasitic cancellation techniques proposed in literature are verified by

the corresponding PEEC-BIM simulations, it is shown that the PEEC-BIM modeling can be used to assess the influence of the *ESL*, *EPC* and mutual coupling cancellation techniques on the improvement of the overall EMI filter behavior. It has to be pointed out that these cancellation techniques have to be carefully implemented in order not to introduce additional negative couplings.

The PEEC-BIM method was implemented in an EMC simulator, GeckoEMC. Good agreement between the GeckoEMC simulations and the transfer function measurements of *L-C* and *C-L-C* filter circuits is achieved in the whole frequency range of interest. It was shown that the impact of the component placement, i.e. PCB layout, on the resulting filter attenuation can be accurately predicted by the developed PEEC-based modeling method. As a result, such an EMC modeling environment represents a useful tool for virtual prototyping of EMI filters and power converter systems, speeding up the design process and allowing engineers to build good EMC designs without wide practical experience.

APPENDIX
THE PEEC METHOD FORMULAS

The PEEC numerical technique is derived from total electric field integral equation (EFIE) (A.1) and the continuity equation of electrical charges (A.2). The system of integral Maxwell equations (A.1) - (A.2) is solved for the unknown volume current distribution $\vec{J}(\vec{r},\omega)$ and the electric charge distribution $\rho(\vec{r},\omega)$, observing a set of conductors occupying the volume υ' that is characterized by the permittivity ϵ_0 and permeability μ_0 of free space.

$$KVL: 0 = \underbrace{\frac{\vec{J}(\vec{r},\omega)}{\sigma}}_{\text{term 1}} + \underbrace{j\omega \cdot \vec{A}(\vec{r},\omega)}_{\text{term 2}} + \underbrace{\nabla\phi(\vec{r},\omega)}_{\text{term 3}} - \underbrace{\vec{E}_{\mathrm{S}}}_{\text{term 4}} \tag{A.1}$$

$$KCL: \nabla \cdot \vec{J}(\vec{r},\omega) + j\omega \cdot \rho(\vec{r},\omega) = 0 \tag{A.2}$$

where $\vec{A}(\vec{r},\omega)$ (A.3) represents the magnetic vector potential characterizing the electric current volume density $\vec{J}(\vec{r})$ and ϕ (A.4) represents the electric scalar potential produced by the free electric charges $\rho(\vec{r},\omega)$ existing in the observed volume υ',

$$\vec{A}(\vec{r},\omega) = \mu_0 \int_{\upsilon'} \vec{J}(\vec{r},\omega) G(\vec{r},\vec{r'})\, \mathrm{d}\upsilon' \tag{A.3}$$

$$\phi(\vec{r},\omega) = \frac{1}{\epsilon_0} \int_{\upsilon'} \rho(\vec{r},\omega) G(\vec{r},\vec{r'})\, \mathrm{d}\upsilon' \tag{A.4}$$

defined by means of the full-wave Green's function $G(\vec{r},\vec{r'})$,

$$G(\vec{r},\vec{r'}) = \frac{e^{-j\beta R}}{4\pi R}, R = |\vec{r} - \vec{r'}|, \beta = \frac{\omega}{c}. \tag{A.5}$$

The result of the PEEC discretization procedure of the modeled conductors, is a set of PEEC cells which can be further defined as PEEC volume cells and PEEC surface cells. The equivalent electrical circuit description is derived by integrating (A.1) separately over all PEEC volume cells, which leads to a set of N_{V} Kichhoff's voltage law equations, that can be written in a matrix form as

$$0 = \underbrace{\mathbf{R} \cdot \mathbf{I}}_{\text{term 1}} + \underbrace{j\omega\mathbf{L} \cdot \mathbf{I}}_{\text{term 2}} + \underbrace{\mathcal{A} \cdot \mathbf{V}}_{\text{term 3}} - \underbrace{\mathbf{V}_{\mathrm{S}}}_{\text{term 4}}. \tag{A.6}$$

The enumerated terms 1-4 in (A.6) correspond respectively to the terms 1-4 in (A.1). The first term of (A.1) can be interpreted as the resistive voltage drop (Joule's losses) along the PEEC volume cells $\Delta\mathbf{V}_{\mathrm{R}}$, the second term represents the inductive voltage drop due to the change of current within the PEEC volume cells $\Delta\mathbf{V}_{\mathrm{L}}$, the third term is the potential difference between the PEEC nodes originating from the electric charges of the PEEC nodes, and the last term $\Delta\mathbf{V}_{\mathrm{S}}$ is the voltage induced in the PEEC volume cells by the external sources. Accordingly, the Joules losses are expressed via the resistance matrix $\mathbf{R} = [R_{i,i}], i \in \{1 \dots N_{\mathrm{V}}\}$, the inductive effect via the inductance matrix $\mathbf{L} = [L_{i,j}], (i,j) \in \{1 \dots N_{\mathrm{V}}\}$, and the capacitive effect by the matrix of potentials $\mathbf{P} = [P_{i,j}], (i,j) \in \{1 \dots N_{\mathrm{S}}\}$, i.e. the relation between the charge at PEEC nodes $\mathbf{Q}$ and the PEEC nodes potentials $\mathbf{V}$ is given by the $\mathbf{P}$ matrix (A.7). Similarly, the continuity equation of electrical charges (A.2) is transformed to Kichhoff's current law (KCL) equations defined at the PEEC nodes (A.8). The matrix $\mathcal{A}$ is the connectivity matrix, which describes the connection of the PEEC volume cells via the common PEEC nodes.

$$\mathbf{V} = \mathbf{P} \cdot \mathbf{Q} \tag{A.7}$$

$$\mathcal{A}^T \cdot \mathbf{I} + \mathrm{j}\omega \cdot \mathbf{Q} = 0 \tag{A.8}$$

REFERENCES

[1] M. N. Yazar, "Civilian EMC standards and regulations," *IEEE Trans. Electromagn. Compat.*, vol. 21, no. 1, pp. 2–8, 1979.

[2] H. Chung, S. Y. R. Hui, and K. K. Tse, "Reduction of power converter EMI emission using soft-switching technique," *IEEE Trans. Electromagn. Compat.*, vol. 40, no. 3, pp. 282–287, 1998.

[3] F. Lin and D. Chen, "Reduction of power supply EMI emission by switching frequency modulation," *IEEE Trans. Power Electron.*, vol. 3, no. 1, pp. 132–137, 1994.

[4] L. Rossetto, S. Buso, and G. Spiazzi, "Conducted EMI issues in a 600-W single-phase boost PFC design," *IEEE Trans. Ind. Appl.*, vol. 36, no. 2, pp. 578–585, 2000.

[5] K. Mainali and R. Oruganti, "Conducted EMI mitigatin techniques for switch-mode power converters: A survey," *IEEE Trans. Power Electron.*, vol. 25, no. 9, pp. 2344–2356, 2010.

[6] S.-P. Weber, E. Hoene, S. Guttowski, J. John, and H. Reichl, "Predicting parasitics and inductive coupling in EMI-filters," in *Proc. IEEE 21st Annual Applied Power Electronics Conf. and Exposition (APEC 2006)*, vol. 1, 2006, pp. 1157–1160.

[7] M. L. Heldwein, "EMC filtering of three-phase PWM converters," Ph.D. dissertation, Swiss Federal Institute of Technology (ETH), 2007.

[8] S. Wang, F. Lee, and W. G. Odendaal, "Characterization and parasitic extraction of EMI filters using scattering parameters," *IEEE Trans. Power Electron.*, vol. 20, no. 2, pp. 502–510, 2005.

[9] E. Hoene, "EMC in power electronics," in *Proc. 5th International Conference on Integrated Power Systems (CIPS 2008)*, 2008, pp. 1–5.

[10] T. De Oliveira, J. Schanen, J. Guichon, and L. Gerbaud, "Automatic layout optimization of an EMC filter," in *Proc. of the 2nd IEEE Energy Conversion Congress and Exposition, (ECCE 2010)*, 2010, pp. 2679–2685.

[11] I. F. Kovacevic, T. Friedli, A. Muesing, and J. W. Kolar, "PEEC-based virtual design of EMI input filters," in *Proc. IEEE Energy Conversion Congress and Exposition (ECCE 2011)*, 2011, pp. 1935–1941.

[12] ——, "Electromagnetic modeling of EMI input filters," in *Proc. 7th International Conference on Integrated Power Systems (CIPS 2012)*, no. 38-47, 2012.
[13] ——, "A full PEEC modeling of EMI filter inductors in frequency domain," in *presented at the COMPUMAG Conference (COMPUMAG 2011), Sydney, Australia*, no. ID 193, 2011.
[14] I. F. Kovacevic, A. Muesing, and J. W. Kolar, "An extension of PEEC method for magnetic materials modeling in frequency domain," *IEEE Transactions on Magnetics*, vol. 47, no. 5, pp. 910–913, 2011.
[15] C. Jettanasen, F. Costa, and C. Vollaire, "Common-Mode emissions measurements and simulation in variable-speed drive systems," *IEEE Trans. Power Electron.*, vol. 24, no. 11, pp. 2456–2464, 2009.
[16] S. Wang, F. Lee, D. Y. Chen, and W. G. Odendaal, "Effects of parasitic parameters on EMI filter performance," *IEEE Trans. Power Electron.*, vol. 19, no. 3, pp. 869–877, 2004.
[17] T. C. Neugebauer, "Advanced filters and components for power application," Ph.D. dissertation, Massachusetts Institute of Technology (MIT), USA, 2004.
[18] B. J. Pierquet, T. C. Neugebauer, and D. J. Perreault, "A fabrication method for integrated filter elements with inductance cancellation," *IEEE Trans. Power Electron.*, vol. 24, no. 3, pp. 838–848, 2009.
[19] ——, "Inductance compensation of multiple capacitors with application to common- and differential-mode filters," *IEEE Trans. Power Electron.*, vol. 21, no. 6, pp. 1815–1824, 2006.
[20] S. Wang, F. Lee, and J. D. Van Wyk, "A study of integration of parasitic cancellation techniques for EMI filter design with discrete components," *IEEE Trans. Power Electron.*, vol. 23, no. 6, pp. 3094–3102, 2008.
[21] S. Wang, C. R., J. D. Van Wyk, F. Lee, and W. G. Odendaal, "Developing parasitic cancellation technologies to improve EMI filter performance for switching mode power supplies," *IEEE Trans. Electromagn. Compat.*, vol. 47, no. 4, pp. 921–929, 2005.
[22] S. Wang, F. Lee, W. G. Odendaal, and J. D. Van Wyk, "Improvement of EMI filter performance with parasitic coupling cancellation," *IEEE Trans. Power Electron.*, vol. 20, no. 5, pp. 1221–1228, 2005.
[23] H. Chen, Z. Qian, Z. Zeng, and C. Wolf, "Modeling of parasitic inductive couplings in a Pi-shaped common mode EMI filter," *IEEE Trans. Electromagn. Compat.*, vol. 50, no. 1, pp. 71–79, 2008.
[24] H.-D. Bruns, C. Schuster, and H. Singer, "Numerical electromagnetic field analysis for EMC problems," *IEEE Trans. Electromagn. Compat.*, vol. 49, no. 2, pp. 253–262, 2007.
[25] A. E. Ruehli, "Equivalent circuit models for three-dimensional multiconductor systems," *IEEE Trans. Microw. Theory Tech.*, vol. 22, no. 3, pp. 216–221, 1974.
[26] J. Ekman, "Electromagnetic modeling using the Partial Element Equivalent Circuit Method," Ph.D. dissertation, Computer Science and Electrical Engineering / EMC Center, Lulea University of Technology, Sweden, 2003. [Online]. Available: http://staff.www.ltu.se/ jekman/Pres/PhDThesis.pdf
[27] A. Muesing, J. Ekman, and J. W. Kolar, "Efficient calculation of non-orthogonal partial elements for the PEEC method," *IEEE Trans. Magn.*, vol. 45, no. 3, pp. 1140–1143, 2009.
[28] Gecko-Research. [Online]. Available: http://www.gecko-research.com/geckoemc.html
[29] T.-S. Tran, G. Meunier, P. Labie, and J. Aime, "Comparison of FEM-PEEC coupled method and Finite-Element method," *IEEE Trans. Magn.*, vol. 46, no. 4, pp. 996–999, 2010.
[30] E. Hoene, A. Lissner, S. Weber, S. Guttowski, W. John, and H. Reichl, "Simulating electromagnetic interactions in high power density inverters," in *Proc. of the 36th IEEE Power Electronics Specialists Conf. (PESC 1995)*, 2005, pp. 1665–1670.
[31] A. Domurat-Linde and E. Hoene, "Analysis and reduction of radiated EMI of power modules," in *Proc. of the 7th International Conference on Integrated Power Electronics Systems, (CIPS 2012)*, 2012, pp. 1 – 6.
[32] B. Stube, B. Schroeder, E. Hoene, and A. Lissner, "A novel approach for EMI design of power electronics," in *Proc. of Design, Automation and Test in Europe, (DATE 2008)*, 2008, pp. 170 – 175.
[33] J.-L. De Oliveira, T.and Schanen, J.-M. Guichon, and L. Gerbaud, "Optimal stray magnetic couplings for EMC filters," in *Proc. of IEEE Energy Conversion Congress and Exposition (ECCE 2011)*, 2011, pp. 2693 – 2700.
[34] R. R. Wang, "High power density and high temperature converter design for transportation applications," Ph.D. dissertation, The Virginia Polytechnic Institute and State University, 2012.
[35] I. F. Kovacevic, T. Friedli, A. Muesing, and J. W. Kolar, "Full PEEC modeling of EMI filter inductors in the frequency domain," *IEEE Transactions on Magnetics*, submitted for publication.
[36] Y. Massoud, J. Wang, and J. White, "Accurate inductance extraction with permeable materials using qualocation," in *Technical Proc. of the International Conference on Modeling and Simulation of Microsystems*, 1999, pp. 697 – 700.
[37] OMICRON LAB. [Online]. Available: http://www.omicron-lab.com/bode-100.html
[38] Vacuumscmelze GmbH&Co. Nanocrystalline VITROPERM EMC Products.
[39] Magnetics. [Online]. Available: http://www.mag-inc.com/
[40] Micrometals. [Online]. Available: http://www.micrometals.com
[41] EPCOS. [Online]. Available: http://www.epcos.com/
[42] S. Wang, F. Lee, and W. Odendaal, "Single layer iron powder core inductor model and its effect on boost PFC EMI noise," in *Proc. IEEE 34th Annual Power Electronics Specialist Conference (PESC 2003)*, vol. 2, 2003, pp. 847–852.
[43] A. Massarini, M. Kazimierczuk, and G. Grandi, "Lumped parameter models for single- and multiple-layer inductors ," in *Proc. IEEE 27th Annual Power Electronics Specialists Conference (PESC 1996)*, vol. 1, 1996, pp. 295–301.
[44] J. Biela and K. J. W, "Using transformer parasitics for resonant converters - A review of the calculation of the stray capacitance of transformers," *IEEE Transactions on Industry Applications*, vol. 44, no. 1, pp. 223–233, 2008.
[45] R. Wang, D. Boroyevich, H. Blanchette, and P. Mattavelli, "High power density EMI filter design with consideration of self-parasitic," in *Proc of the 27th Annual IEEE Applied Power Electronics Conference and Exposition (APEC 2012)*, 2012, pp. 2285 – 2289.
[46] S.-P. Weber, M. Schinkel, E. Hoene, S. Guttowski, W. John, and H. Reichl, "Radio frequency characteristics of high power common-mode chokes," in *Proc. 16th International Zurich Symposium on Electromagnetic Compatibility (EMC Zuerich 2005)*, vol. 1, 2005, pp. 507–510.
[47] J. Ekman, G. Antonini, and A. Orlandi, "3D PEEC capacitance calculations," in *Proc. IEEE International Symposium on Electromagnetic Compatibility*, vol. 2, 2003, pp. 630–635.
[48] V. Yurschevich, S. Lomov, and J. Jankovskis, "Measurement of self-capacitance for windings on high-permeability ferrite cores," *Measurement Science Review*, vol. 1, no. 1, pp. 219–222, 2001.
[49] D. Zhang, "Permeability enhancement by induced displacement current in magnetic material with high permittivity," *Journal of Magnetism and Magnetic Materials*, vol. 313, no. 1, pp. 47–51, 2007.
[50] S. Wang, F. Lee, and J. Van Wyk, "Design of inductor winding capacitance cancellation for EMI suppression," *IEEE Trans. Power Electron.*, vol. 21, no. 6, pp. 1825–1832, 2006.

Ivana Kovacevic (SM'10) graduated from the University of Belgrade, Serbia, Faculty of Electrical Engineering, Department for Electronics, in 2006 (with honors). In June 2007 she joined the Power Electronic Systems Laboratory at the the Swiss Federal Institute of Technology (ETH), Zurich, Switzerland as a postgraduate student. She received the M.Sc. degree in electrical engineering and information technology and Ph.D. degree from ETH Zurich in 2008 and 2012, respectively, focusing on lifetime modeling of power modules and 3D electromagnetic modeling of Electromagnetic Interference (EMI) Filters. She is currently working as a Postdoctoral Assistant in the Power Electronic Systems Laboratory at ETH Zurich. Her research activities are focused on multi-domain modeling and optimization of power electronics systems and components. She received the Rita Trowbridge Prize from the International Compumag Society for a presented paper at the COMPUMAG Conference 2011.

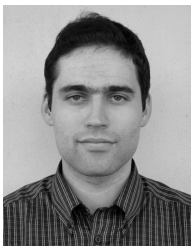

Thomas Friedli (M'09) received his M.Sc. degree (Hons.) in electrical engineering and information technology and his Ph.D. from the Swiss Federal Institute of Technology (ETH) Zurich, in 2005 and 2010, respectively.
From 2006 to 2011, he was with the Power Electronic Systems Laboratory, ETH Zurich, Switzerland where he performed research on current source and matrix converter topologies using silicon carbide power semiconductors, active three-phase PFC rectifiers, and conducted electro-magnetic interference. Since 2012, he has been with ABB Switzerland Ltd. He is currently involved in the research and development of power electronics and medium voltage drives for traction converter systems. His research interests are in the areas of high-efficiency power electronic systems and their control, three-phase power converters, electro-magnetic interference, and applications of wide band-gap power devices. Dr. Friedli received the 1st Prize Paper Award of the IEEE IAS IPCC in 2008 and the IEEE TRANSACTIONS ON INDUSTRY APPLICATIONS Prize Paper Award in 2009.

Andreas Muesing (M'12) received his degree in Physics at the Ruprecht-Karls-University in Heidelberg, Germany in 2005. From 2006 to 2012, he conducted his PhD at the Power Electronic Systems Laboratory, ETH Zurich, Switzerland, where his reseach was focused on numerical simulations of power electronics systems. Andreas Msing founded the company Gecko-Research GmbH, which he is leading as CEO since 2010.

Johann W. Kolar (F'10) received his M.Sc. and Ph.D. degree (summa cum laude / promotio sub auspiciis praesidentis rei publicae) from the University of Technology Vienna, Austria. Since 1982 he has been working as an independent international consultant in close collaboration with the University of Technology Vienna, in the fields of power electronics, industrial electronics and high performance drives. He has proposed numerous novel converter topologies and modulation/control concepts, e.g.the VIENNA Rectifier, the SWISS Rectifier, and the three-phase AC-AC Sparse Matrix Converter. Dr. Kolar has published over 400 scientific papers at main international conferences and over 150 papers in international journals and has filed more than 110 patents. He was appointed Professor and Head of the Power Electronic Systems Laboratory at the Swiss Federal Institute of Technology (ETH) Zurich on Feb. 1, 2001. The focus of his current research is on AC-AC and AC-DC converter topologies with low effects on the mains, e.g. for data centers, More-Electric-Aircraft and distributed renewable energy systems, and on Solid-State Transformers for Smart Microgrid Systems. Further main research areas are the realization of ultra-compact and ultra-efficient converter modules employing latest power semiconductor technology (SiC and GaN), micro power electronics and/or Power Supplies on Chip, multi-domain/scale modeling/simulation and multi-objective optimization, physical model-based lifetime prediction, pulsed power, and ultra-high speed and bearingless motors. He has been appointed an IEEE Distinguished Lecturer by the IEEE Power Electronics Society in 2011. He received 7 IEEE Transactions Prize Paper Awards and 7 IEEE Conference Prize Paper Awards. Furthermore, he received the ETH Zurich Golden Owl Award 2011 for Excellence in Teaching and an Erskine Fellowship from the University of Canterbury, New Zealand, in 2003. He initiated and/or is the founder/co-founder of 4 spin-off companies targeting ultra-high speed drives, multi-domain/level simulation, ultra-compact/efficient converter systems and pulsed power/electronic energy processing. Dr. Kolar is a Fellow of the IEEE and a Member of the IEEJ and of International Steering Committees and Technical Program Committees of numerous international conferences in the field. He is the founding Chairman of the IEEE PELS Austria and Switzerland Chapter and Chairman of the Education Chapter of the EPE Association. From 1997 through 2000 he has been serving as an Associate Editor of the IEEE Transactions on Industrial Electronics and since 2001 as an Associate Editor of the IEEE Transactions on Power Electronics. Since 2002 he also is an Associate Editor of the Journal of Power Electronics of the Korean Institute of Power Electronics and a member of the Editorial Advisory Board of the IEEJ Transactions on Electrical and Electronic Engineering.